Instrumentation Science & Technology
Publication details, including instructions for authors and subscription information:
http://www.tandfonline.com/loi/list20

AUTOMATIC INSPECTION SYSTEM FOR DEFECTS OF PRINTED ART TILE BASED ON TEXTURE FEATURE ANALYSIS

Shih-Wei Yang [a] , Chern-Sheng Lin [b] , Shir-Kuan Lin [a] & Yung-Chin Tseng [b]

[a] Institute of Electrical and Control Engineering, National Chiao Tung University , Hsinchu , Taiwan

[b] Department of Automatic Control Engineering , Feng Chia University , Taichung , Taiwan

Accepted author version posted online: 02 Sep 2013.Published online: 25 Nov 2013.

To cite this article: Shih-Wei Yang , Chern-Sheng Lin , Shir-Kuan Lin & Yung-Chin Tseng (2014) AUTOMATIC INSPECTION SYSTEM FOR DEFECTS OF PRINTED ART TILE BASED ON TEXTURE FEATURE ANALYSIS, Instrumentation Science & Technology, 42:1, 59-71, DOI: 10.1080/10739149.2013.836659

To link to this article: http://dx.doi.org/10.1080/10739149.2013.836659

Instrumentation Science and Technology, 42:59–71, 2014

ISSN: 1073-9149 print/1525-6030 online
DOI: 10.1080/10739149.2013.836659

Taylor & Francis
Taylor & Francis Group

AUTOMATIC INSPECTION SYSTEM FOR DEFECTS OF PRINTED ART TILE BASED ON TEXTURE FEATURE ANALYSIS

Shih-Wei Yang,[1] Chern-Sheng Lin,[2] Shir-Kuan Lin,[1] and Yung-Chin Tseng[2]
[1]*Institute of Electrical and Control Engineering, National Chiao Tung University, Hsinchu, Taiwan*
[2]*Department of Automatic Control Engineering, Feng Chia University, Taichung, Taiwan*

□ *An automatic inspection system of printed art tile defects is reported in this artucke. After calculating eight defect features of art tile using the gray level co-occurrence matrix and the average R, G, B values of a defective area, the results were input into a backward propagation neural network for training the defect classifier. During inspection, the proposed system compared the inspected image with a standard image and removed noise by an erosion operation in order to preliminarily determine whether the art tile had defects. For the defective art tile images, the proposed classifier successfully identified four types of common printing defects. The proposed algorithm had an average recognition rate of 90%, suggesting that the recognition accuracy is good, and only requires 1–2 s to inspect an art tile with the size of 15 × 15 cm^2. The inspection speed is faster than the conventional manual inspection, and recognition results are more stable. The proposed system can reduce the risk of error caused by the long duration of manual inspection, and thus, can reduce manufacturing costs.*

Keywords defect classifier, gray level co-occurrence matrix, printed art tile

INTRODUCTION

In recent years, the demand for printed art tile has diversified, resulting in higher requirements for printing quality. However, in the printing process, the damage of machine components often cause defects on tiles, which can be divided into the following four types: (1) scratches, caused by contact between inkjet head and tiles; (2) horizontal blank defects, caused by obstruction of inkjet heads; (3) ink-leaking defects, due to damage of the back pressure module of the inkjet head, the inkjet head is unable to absorb the ink; and (4) particle defects, caused by dust, ink stains, and other foreign matter. The industry currently relies on manual

Address correspondence to Shih-Wei Yang, Institute of Electrical and Control Engineering, National Chiao Tung University, Hsinchu, Taiwan. E-mail: swyang.nctu@msa.hinet.net

inspection for defect detection, which often results in misjudgment or uneven inspection quality.

Some studies relating to tile inspection have been proposed.[1,2] Boukouvalas et al. proposed a tile defect inspection system able to recognize small cracks and spot-like defects in plain white tiles.[3] Lin and Fan designed an automated tile installation quality assurance system, which calculates geometric tile characteristics by a machine vision technique in order to improve tile alignment.[4] Smith and Stamp constructed a tile surface topographic measurement system, where the user sets the initial lighting conditions and calculates tile features for reconstruction of the surface three-dimensional topography.[5] However, some of these methods cannot meet the requirements of in-line inspection and some are not suitable for the detection of print defects in art tiles.

Hence, by integrating image processing techniques[6–10] and modifying the conventional method,[11,12] this study designs an automatic system for defects of printed art tiles, which is suitable for in-line inspection of printed tile defects. After analyzing the art tile texture features through gray level co-occurrence matrix, the analysis results were input into the backward propagation neural network in order to train the defect classifier. The defect classifier was applied in the recognition of various defective tile samples, in order to verify the robustness, accuracy, and practicability of the proposed system.

METHODS OF DEFECT RECOGNITION FOR PRINTED ART TILES

This article inspects and recognizes the most common four types of defects that occur during the printing process: (1) scratches, (2) blank defects, (3) ink leaking, and (4) particle defects. The actual images of the four types of defects are as shown in Figure 1; the defect recognition process will be illustrated in the following subsections.

Denoising Process and Preliminary Recognition of Defects

The system first determined whether the art tile has any defects, and will implement defect recognition of tiles. The system converted the inspected images into grayscale images and conducted image subtraction with the standard image of the tile. After subtraction, binary images often have noise, which cannot be removed by median value filtering; however, the noise can be effectively removed by an erosion operation, as shown in Figure 2. The defective area of the tile is the white block of the binary image, which is often a large area. Hence, this system will recognize the white block of an area (Figure 2d) greater than the preset threshold as a tile defect for further recognition.

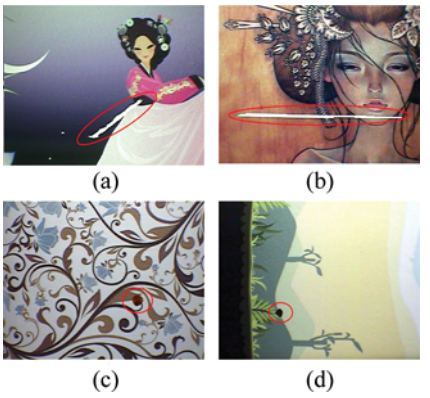

FIGURE 1 Four common defects in art tile printing process: (a) scratch, (b) blank defect, (c) ink leaking, and (d) particle defect. (color figure available online.)

Texture Feature Analysis of Defects in Printed Art Tiles

This article uses the gray level co-occurrence matrix, as proposed by Haralick et al.,[13] to calculate the features of various art tile defects as the basis for recognition. However, considering the high amount of computation of the technique, this study scaled down the defect image size from 640×480 to 320×240, and compressed the grayscale value from 256 levels to 16 levels in order to enhance the recognition speed. To convert the inspected image into the gray level co-occurrence matrix, the relative position of the pixels of the image was determined first. More specifically, i and j are defined as the gray tone value of pixels of $g(u, v)$ and $g(m, n)$, d is the distance between $g(u, v)$ and $g(m, n)$, θ is the angle between $g(u, v)$ and $g(m, n)$, where θ can be 0°, 45°, 90°, or 135°, as shown in Figure 3.

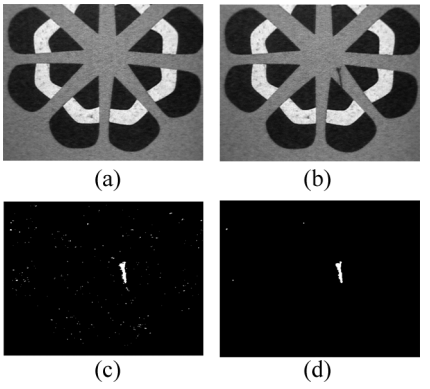

FIGURE 2 Results of denoising process: (a) standard image of art tile, (b) inspected image of art tile, (c) binary image of subtraction result for (a) and (b), and (d) result of erosion operation for (c).

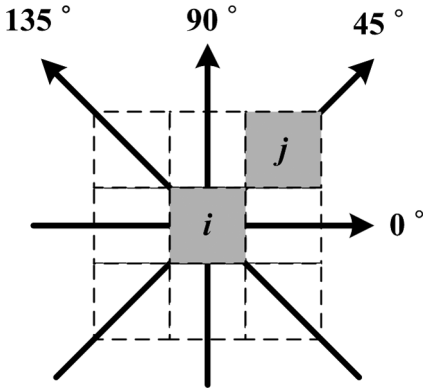

FIGURE 3 Calculation of gray level co-occurrence matrix in four angles.

Regarding the four different angles, the system calculated the occurrence times of gray tone value of i and j of pixels $g(u, v)$ and $g(m, n)$, and the results are represented as $p(i, j|d, \theta)$. Figure 4 shows the gray level co-occurrence matrix result of defective tiles when $d=4$ and $\theta=90°$.

The gray level co-occurrence matrix obtained according to Figure 3 can be further normalized to allow each of the matrix elements to represent the occurrence probability of a gray tone value. The normalized matrix can be obtained by dividing the value of each element of matrix $p(i, j|d, \theta)$ by the summation of all element values:

$$P(i,j|d,\theta) = \frac{p(i,j|d,\theta)}{N}, \tag{1}$$

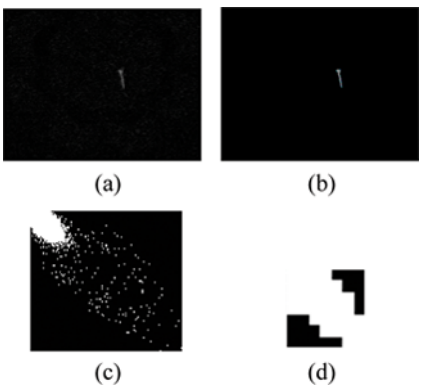

FIGURE 4 Gray level co-occurrence matrix result of defective tile when choosing $d=4$ and $\theta=90°$: (a) original image, (b) compressed image of (a), (c) gray level co-occurrence matrix result of (a), and (d) gray level co-occurrence matrix result of (b). (color figure available online.)

where $P(i, j|d, \theta)$ is the normalized matrix element value and N is the summation of all the element values in the matrix.

Considering the five features in the case of different angles (0°, 45°, 90°, and 135°),[13,14] the texture characteristics of tile defects are analyzed as follows:

P_1: Angular second moment

$$P_1 = \sum_i \sum_j [P(i,j|d,\theta)]^2 \tag{2}$$

P_2: Entropy

$$P_2 = -\sum_i \sum_j P(i,j|d,\theta) \log P(i,j|d,\theta) \tag{3}$$

P_3: Contrast

$$P_3 = \sum_{n=0}^{Ng-1} n^2 \left[\sum_{i=1}^{Ng} \sum_{j=1}^{Ng} P(i,j|d,\theta) \right], \quad |i-j| = n \tag{4}$$

P_4: Correlation

$$P_4 = \frac{\sum_i \sum_j (i \times j) P(i,j|d,\theta) - \mu_x \mu_y}{\sigma_x \sigma_y} \tag{5}$$

P_5: Homogeneity

$$P_5 = \sum_i \sum_j \frac{P(i,j|d,\theta)}{1 + (i-j)^2}, \tag{6}$$

where Ng= (maximum grayscale value of the image − minimum grayscale value of the image) + 1, known as the gray tone value,

$$\mu_x = \sum_i \sum_j i \times P_{nor}(i,j|d,\theta), \sigma_x = \sum_i \sum_j (i-\mu_x)^2 \times P_{nor}(i,j|d,\theta),$$

$$\mu_y = \sum_i \sum_j j \times P_{nor}(i,j|d,\theta), \sigma_y = \sum_i \sum_j (i-\mu_y)^2 \times P_{nor}(i,j|d,\theta).$$

Regarding the above features, this study calculates the average value of the four angles as the texture feature of tile defects. In addition, this study selects the average of R-value, G-value, and B-value, in the defective area

of the original image as the other three features (P_6, P_7, P_8). The total eight types of features are regarded as the texture features of tile defects in each image.

Implementation of Defect Classifier using Backward Propagation Neural Network

The eight art tile defect features are used as the inputs of the multi-layer feed forward neural network in order to train a defect classifier for recognition. The classifier outputs include the corresponding scores of the four defects. The defect with the highest score is the recognition results. This study uses the backward propagation algorithm[15,16] as the learning method of the defect classifier. The concept of the algorithm is to feed back the differences between the desired output and actual output in order to update the weight of each node and reduce errors between the desired output and actual output.

The backward propagation update rule can be represented as:[16,17]

$$w_{ij}^{new} = w_{ij}^{old} + \Delta w_{ij} \tag{7}$$

$$\Delta w_{ij} = \eta \delta_i x_j,$$

where w_{ij}^{new} is the node weight after learning, w_{ij}^{old} is the node weight before learning, Δw_{ij} is the weight change, η is positive and is known as the learning constant, δ_i is the learning signal, and x_j represents an input eigenvalue or an input of the processing element of the hidden layer.

This study uses the unipolar sigmoid function $a(f) = 1/(1 + e^{-f})$ as the activation function, therefore, the learning signal of the ith node of the output layer corresponding to Eq.(7), $\delta_{o(i)}$, can be represented as:

$$\delta_{o(i)} = y_i(1 - y_i)[d_i - y_i] \tag{8}$$

where y_i is the actual output of ith node in the output layer and d_i is the corresponding desired output.

Similarly, corresponding to Eq. (7), the qth node of the hidden layer's learning signal $\delta_{h(q)}$ can be represented as:

$$\delta_{h(q)} = z_q(1 - z_q) \sum_i \delta_{o(i)} w_{iq}, \tag{9}$$

where z_q is the output of qth node in the hidden layer and w_{iq} is the weight from the qth node in the hidden layer to the ith node in the output layer.

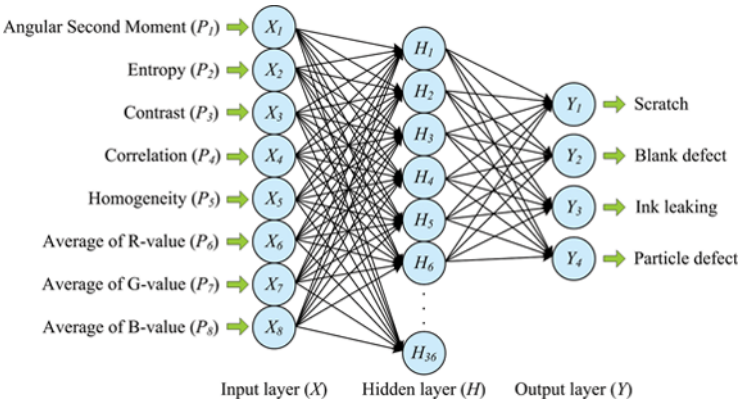

FIGURE 5 Neural network architecture of the proposed defect classifier. (color figure available online.)

According to Eqs. (7)–(9), the weight of each node of the defect classifier can be updated to achieve the purpose of learning.

This study used MATLAB to realize the above algorithm. The defect classifier had a three-layered network architecture. The input layer had eight defect features and the hidden layer has 36 nodes. The output layer had four output scores corresponding to the four types of defects, as shown in Figure 5. The learning times were set as 6,000 times, when the root mean square error of all the actual outputs and desired outputs is smaller than the preset threshold value, it means that the art tile defect classifier has completed learning.

RESULTS AND DISCUSSION

Experimental Framework of the Proposed System

This study collected 200 defective tiles as the training samples, and computed 8 features, including angular second moment, entropy, contrast, correlation, homogeneity, and R, G, B average values of the defective area as the inputs of backward propagation neural network. When the root mean square error of the actual outputs and desired outputs was smaller than the preset threshold value, it meant the art tile defect classifier had completed learning and can be used for recognition of the four common types of defects in ink jet printing. The framework of the proposed art tile defect inspection system is shown in Figure 6.

Each art tile is transmitted via a conveyor under the CCD camera. After capturing the image by the camera, the subtraction of the standard image and image under test is conducted. Then, by analyzing the binary results of

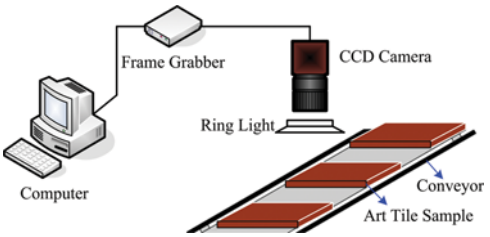

FIGURE 6 Framework of the proposed system. (color figure available online.)

image subtraction, if the area of the white blocks is greater than the preset threshold, it meant the tile was very likely to have defects, and was recognized by the defect classifier. If there were no defects, it captured the next image. The complete inspection process is shown in Figure 7.

Defect Recognition Results and Discussion

The selection of different pixel distance d and angle θ will result in different results of gray level co-occurrence matrix, affecting the accuracy of recognition results. Hence, this study selected two samples for each of the four types of defects (scratch, blank defect, ink leaking, particle defect), described trends of gray level co-occurrence matrix features, pixel distance d and angle θ to summarize the optimal d and θ values of the recognition effect. Figure 8 demonstrates the trends of features (angular second moment (P_1), contrast (P_3), and correlation (P_4)) and d, θ.

As shown in Figure 8, when $d \geq 4$, the trends of change in various features stabilized, and the corresponding ranges of features have obvious differences. However, the features have no significant differences in the case of four angles of 0°, 45°, 90°, and 135°. Obviously, the features were not significantly affected by the angle. In addition, the change in the trends of P_2, P_5 and d, θ have the same rules. If pixel distance d is of a greater value, there were a large number of pixels not participating in the computation of gray level co-occurrence matrix, resulting in the loss of numerous image details. Hence, this method calculated features by setting pixel distance at $d = 4$, and uses the average of the features of the four angles as the inputs of the neural network in order to distinguish different tile defects.

By inputting the features of art tiles into the trained defect classifier, a group of output vectors were obtained, which included the corresponding scores of the four defects in the range of 0 to 1. The defect with the highest score is the recognition result. In other words, if the maximum output value corresponds to the maximum value of the target output vector, it means the defect recognition is successful; otherwise, it is a recognition failure. Table 1 illustrates the input features of 12 art tile samples. Groups 1–3

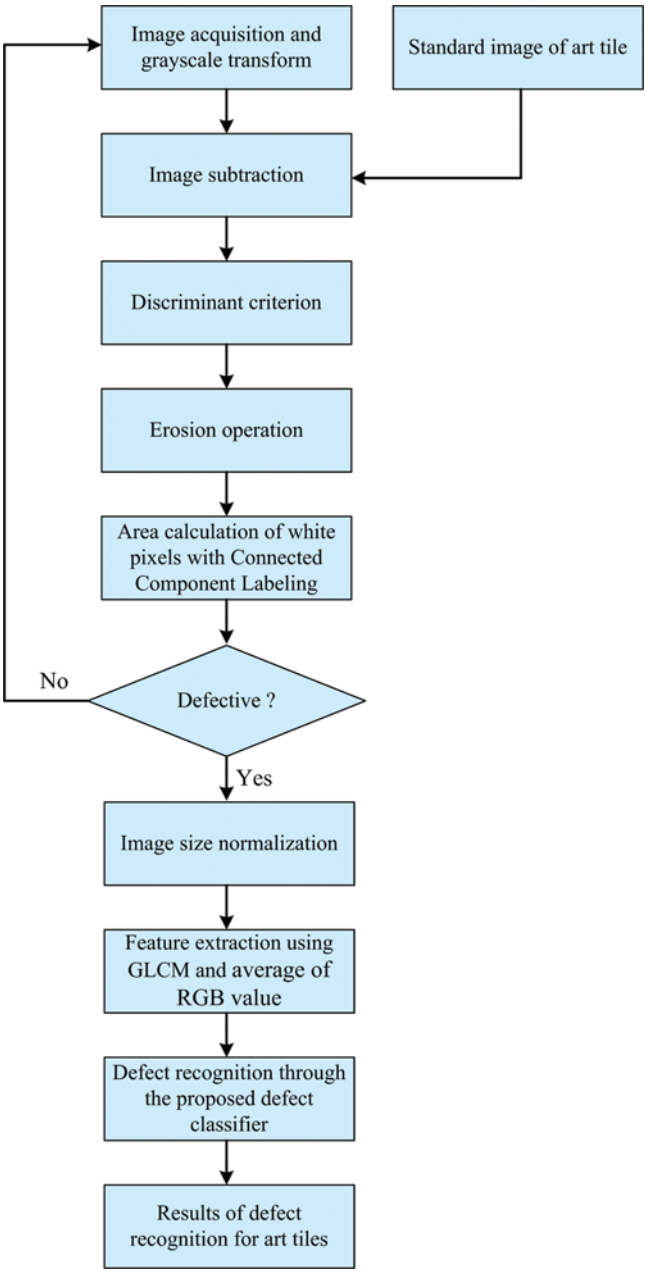

FIGURE 7 Flowchart of the proposed defect recognition method for art tiles. (color figure available online.)

are tile samples of scratch defects. Groups 4–6 are tile samples of blank defects, Groups 7–9 are tile samples of ink leaking defects, and Groups 10–12 are tile samples of particle defects. Table 2 illustrates the output

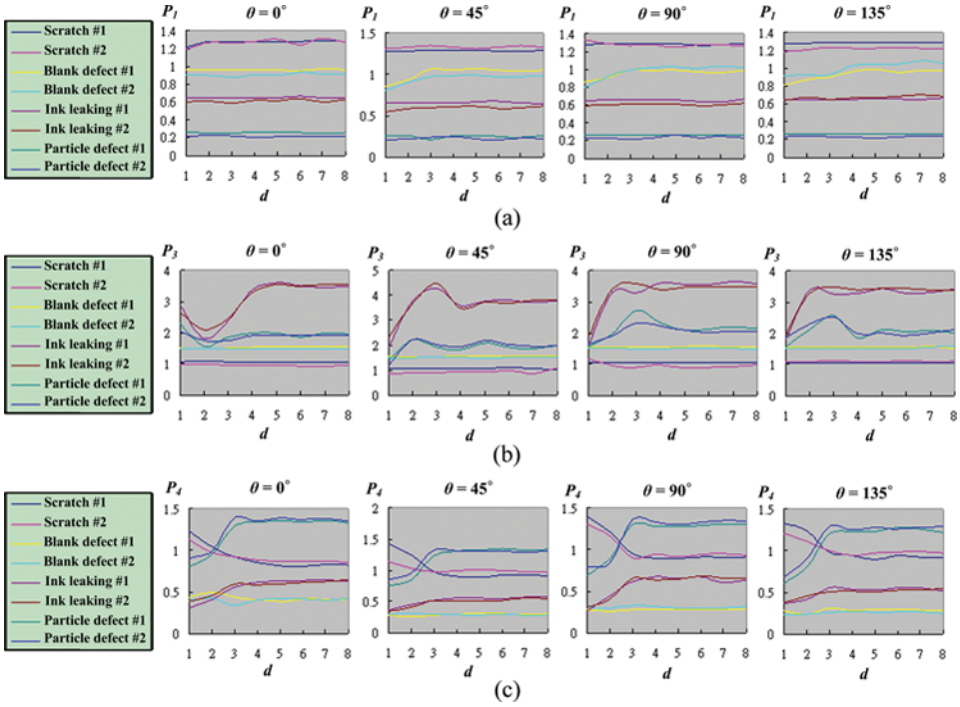

FIGURE 8 (a) Trends of feature P_1 and d, θ, (b) trends of feature P_3 and d, θ, and (c) trends of feature P_4 and d, θ. (color figure available online.)

vectors of 12 art tile samples (output scores). As shown in Table 2, as the highest score of sample 1 corresponds to the scratch defects, sample 1 is recognized as a scratch defect, indicating recognition success. Similarly, samples 2–12 are examples of recognition success.

TABLE 1 Input Features of 12 Art Tile Samples

Sample	P_1	P_2	P_3	P_4	P_5	P_6	P_7	P_8
1	1.256	0.070	1.049	0.803	1.298	254.938	206.036	206.024
2	1.235	0.072	1.048	0.865	1.282	252.593	197.499	197.524
3	1.216	0.071	1.065	0.888	1.228	255	212.563	212.314
4	0.892	0.178	1.512	0.392	1.043	254.513	191.089	191.524
5	0.925	0.153	1.592	0.386	1.035	254.478	203.042	203.491
6	0.928	0.164	1.527	0.325	1.062	254.123	197.248	198.04
7	0.653	0.444	3.456	0.598	0.619	42.508	226.824	18.081
8	0.601	0.412	3.512	0.602	0.613	251.348	225.448	17.026
9	0.643	0.438	3.524	0.543	0.638	123.449	96.082	97.908
10	0.273	0.755	1.995	1.295	0.283	56.486	19.280	21.788
11	0.214	0.764	1.999	1.255	0.265	59.595	17.477	19.483
12	0.229	0.740	1.910	1.264	0.251	56.576	15.408	16.969

TABLE 2 Output Vectors of 12 Art Tile Samples

Sample	Target Output	Actual Output			
		Scratch	Blank Defect	Ink Leaking	Particle Defect
1	[1000]	0.724	0.302	0.157	0.145
2	[1000]	0.819	0.349	0.121	0.126
3	[1000]	0.837	0.165	0.218	0.178
4	[0100]	0.126	0.813	0.140	0.053
5	[0100]	0.323	0.772	0.112	0.096
6	[0100]	0.196	0.744	0.199	0.086
7	[0010]	0.211	0.126	0.811	0.173
8	[0010]	0.208	0.155	0.790	0.167
9	[0010]	0.228	0.175	0.801	0.164
10	[0001]	0.143	0.087	0.111	0.798
11	[0001]	0.175	0.176	0.129	0.789
12	[0001]	0.196	0.164	0.124	0.804

This study uses recognition rate to evaluate the recognition effect, where recognition rate R can be defined as:

$$R = \frac{\text{Numbers of correctly detected samples}}{\text{Numbers of all samples}} \times 100\%. \tag{10}$$

The proposed defect classifier was used to recognize 1,200 art tile samples, and each defect group contained 300 samples. Table 3 illustrates the corresponding recognition rates of various types of defects.

According to Table 3, the proposed defect recognition method had an average recognition rate of 90%; thus, the recognition effect is accurate and is in line with the production standards of the industry. It takes 1–2 s to detect an art tile with the size of $15 \times 15\,\text{cm}^2$, and hence the inspection rate was faster than the conventional manual inspection. The recognition result is more stable and low in cost. However, it is worth pointing out that the proposed method is suitable for the inspection of tile defects and other similar printed materials during the ink jet printing process, while it may not be suitable for defects of other manufacturing processes. In other words, if the type of defects or process is changed, the defect classifier

TABLE 3 Recognition Results of 1200 Art Tile Samples

	Scratch	Blank Defect	Ink Leaking	Particle Defect
Number of samples	300	300	300	300
Recognition success	268	271	275	283
Recognition failure	32	29	25	17
Recognition rate (%)	89.33	90.33	91.66	94.33

framework should be modified to fit the new defect or sample, which is the inspection limitation of the proposed system.

CONCLUSIONS

This article proposed a recognition system for defects of printed art tiles, consisting of a lighting module, a CCD camera, an image capture card, and a computer. By using the texture features of gray level co-occurrence matrix and mean R, G, B values of defective area as eight art tile defect features, and inputting the results into a backward propagation neural network for the training of the defect classifier, the proposed system recognized the most common defects during the ink jet printing process. According to the results, the proposed algorithm had an average 90% recognition rate, suggesting that the recognition effect is suitable. It takes −2 s to inspect an art tile, which is faster and more stable than the conventional manual inspection. However, it should be noted that if the type of defects or process changes, the defect classifier framework should be readjusted to fit the new inspection sample, which is a limitation of the proposed system.

ACKNOWLEDGMENT

This work was sponsored by the National Science Council under Grant No. NSC 102-2221-E-009-064 and NSC 101-2221-E-035-039-MY2.

REFERENCES

1. Kopar, T.; Ducman, V. Low-vacuum SEM analyses of ceramic tiles with emphasis on glaze defects characterization. *Mater. Charact.* **2007**, *58*(11–12), 1133–1137.
2. Eren, E.; Kurama, S.; Solodov, I. Characterization of porosity and defect imaging in ceramic tile using ultrasonic inspections. *Ceram. Int.* **2012**, *38*(3), 2145–2151.
3. Boukouvalas, C.; Natale, F. D.; Toni, G. D.; Kittler, J.; Marik, R.; Mirmehdi, M.; Petrou, M.; Roy, P. L.; Salgari, R.; Vernazza, G. ASSIST: Automatic system for surface inspection and sorting of tiles. *J. Mater. Process Tech.* **1998**, *82*(1–3), 179–188.
4. Lin, K. L.; Fang, J. L. Applications of computer vision on tile alignment inspection. *Automat. Constr.* **2013**, *35*, 562–567.
5. Smith, M. L.; Stamp, R. J. Automated inspection of textured ceramic tiles. *Comput. Ind.* **2000**, *43*(1), 73–82.
6. Minamisawa, R. A.; Santos, L. E. R.; Parada, M. A.; Daghastanli, K. R. P.; Ciancaglini, P. Digital image analysis to standardize a photometric method in colorimetric quantification. *Instrum. Sci. Technol.* **2007**, *36*(1), 97–104.
7. Song, Q.; Zhang, G.; Qiu, Z. Drop growth monitoring and drop volume measurement based on image drop analysis with CCD. *Instrum. Sci. Technol.* **2003**, *31*(1), 1–13.
8. Todtong, Y.; Kaewrawang, A.; Sivaratana, R.; Kruesubthaworn, A.; Thompson, S. M.; Siritaratiwat, A. Thermal image refinement approach for scratches on a magnetic disk evaluated at various angles. *Instrum. Sci. Technol.* **2013**, *41*(4), 365–381.

9. Blagojevic, B.; Sirok, B.; Hocevar, M. Monitoring and control of quality of the primary layer of mineral wool on a disc spinning machine. *Instrum. Sci. Technol.* **2003**, *31*(1), 63–75.
10. Fisher, M.; Feller, L.; Schechter, I. Examination of oral tissues by fourier transform spectral imaging fluorescence. *Instrum. Sci. Technol.* **2001**, *29*(1), 11–16.
11. Lin, C. S.; Liao, Y. C.; Lay, Y. L.; Lee, K. C.; Yeh, M. S. High-speed TFT LCD defect detection system with genetic algorithm. *Assembly Autom.* **2008**, *28*(1), 69–76.
12. Lin, C. S.; Kuo, J.; Lin, C. C.; Lay, Y. L.; Shei, H. J. Automatic inspection and strategy for surface defects in PI coating process of TFT-LCD panels. *Assembly Autom.* **2011**, *31*(3), 244–250.
13. Haralick, R. M.; Shanmugam, K.; Dinstein, I. Textural features for image classification. *IEEE T. Syst. Man Cyb.* **1973**, *3*, 610–621.
14. Sutton, R. N.; Hall, E. L. Texture measures for automatic classification of pulmonary disease. *IEEE T. Comput.* **1972**, *C-21*, 667–676.
15. Rumelhart, D. E.; Hinton, G. E.; Williams, R. J. Learning representations by back-propagating errors. *Nature* **1986**, *323*, 533–536.
16. Lin, C. T.; Lee, C. S. G. *Neural Fuzzy Systems: A Neuro-Fuzzy Synergism to Intelligent Systems*; Prentice Hall: Englewood Clifss, NJ, 1996.
17. Lin, C. T.; Lee, C. S. G. Neural-network-based fuzzy logic control and decision system. *IEEE T. Comput.* **1991**, *40*(12), 1320–1336.